Effect of (Ti:B) atomic ratio on mechanical properties of TiB_2-Fe composites “in situ” fabricated via Self-propagating High-temperature Synthesis

Marta Ziemnicka-Sylwester[1, a]*, Li Gai[1, 2, b], Seiji Miura[1, c]

[1] Division of Materials Science and Engineering, Hokkaido University, Kita 13, Nishi 8, Kita-Ku, 060-8628 Sapporo, Japan ph. +81 11 706 6345

[2] Division of Materials of Science and Engineering, University of Science and Technology Beijing, 30 Xueyuan Rd, Haidian, 100083 Beijing, China, ph. +86 10 6233 2893

*Corresponding author. Email: a) marta.zs@emg.hokudai.ac.jp,

b) ligaiustb@gmail.com, c) miura@eng.hokudai.ac.jp

Abstract

The TiB_2-based Fe-matrix cermets with titanium addition (literarily different Ti:B ratio) were fabricated from elemental powders “in situ” using the Self-propagating High-temperature Synthesis method (SHS) under high pressure. The effect of Ti:B ratio on microstructure and phase composition with particular focus on matrix phase were analyzed using X-ray diffraction (XRD) and Wavelength Dispersive Spectroscopy (WDS) for composites with intended 25 vol.% and 35 vol.% of Fe. Moreover, for composites with 35vol% of Fe bending strength and compressive strength were investigated. The compressive strength reached maximum value in material with Ti:B atomic ratio of 0.49, which possessed the highest TiB_2 content and matrix phase consisting of Fe and Fe_2B. However, modulus of rupture (MOR) test indicated that composite with titanium excess (Ti:B atomic ratio of 0.525) was characterized by the highest bending strength, due to successful elimination of Fe_2B intermetallics.

Keywords: Titanium diboride; metal matrix composites; Self-propagating High-temperature Synthesis; modulus of rupture; compressive strength

1. Introduction

Due to extraordinary microhardness (34.0GPa), outstanding tribological properties [1-4], low density (4.52g/cm^3), and good thermal and electrical conductivity [5-9] (60W/m^{-1}K^{-1}) [10], the TiB_2 is considered as a ceramic phase reinforcing advanced cermets [6, 11]. The Young's modulus (E) of 529GPa [3] and transverse rupture strength of even 1500MPa [4] can be reached for nearly monolithic TiB_2 material. Therefore, TiB_2-rich Fe matrix cermets with high volume fraction of TiB_2 are potentially good candidates for machine parts for aerospace, automotive, military, defense, and marine, characterized by high wear resistance as well as for nuclear industry [12-14]. A large damping capacity [15] and predictable fracture mode are desirable for materials used in constructions where unwanted vibrations are induced during operation under irregular loading.

Particular attention is being paid to Al [15-18], Cu or Fe as a toughening binder [2, 6, 8, 11, 19-21], because cermets can be obtained in these systems. In order to fully utilize the high refractoriness of TiB_2 (melting point of 3225°C), Fe is a better candidate for a metallic matrix. Also high E (190-210GPa) [22] and higher hardness of Fe, indicate that better mechanical performance (i.e. damping capacity or high specific modulus) should be expected.

The application of SHS combined with high pressure, revealed to be a useful method for "in-situ" fabrication of TiB_2-based Cu-matrix highly densified cermets [20]. Therefore, the TiB_2-based cermets for those investigations were prepared using SHS under a high pseudo-isostatic pressure, which is one of the most progressive and energy saving methods to obtain TiB_2 and TiB_2-reinforced materials [2, 23-25]. Such method was also used to fabricate the composites used in the previous study [12, 20, 25], especially that the Ti excess can be easily controlled by using the mixtures of elemental (Ti, B, Fe) powders.

However, the production of TiB_2-Fe cermets is a challenge, since the field of crystallization for pseudo-binary TiB_2-Fe system is narrow, as indicated in the

isothermal section of the Fe-B-Ti ternary system [26]. So far, several researchers [22, 24], including the present authors [25], reported the formation Fe_2B boride in the matrix while the intended matrix phase was elemental Fe (=not so easy to understand). Different hypothetical explanations of the unexpected Fe_2B phase were discussed in the recently published papers. For instance, when metallurgical ingredients such as ferroboron or ferrotitanium are used [11, 24], impurities originated from those components, especially C; they are considered as those affecting the formation of Fe_2B precipitates in Fe or steel matrix TiB_2-based cermets [1, 22]. The other authors suggested that it might be caused by not sufficiently fine (coarse) Ti or Fe powders [24]. However, most likely the crystallization of Fe_2B in Fe is caused by Ti dissolving in Fe. Those effects subsequently lead to Ti-deficiency, or excess B which reacts with Fe [1, 22, 25].

The application of structural components in engineering requires both strength and good fracture toughness to avoid catastrophic failure. Since Fe-based compounds and intermetallics are in general brittle, both Fe_2B [13, 27] and Fe_2Ti [9, 28], should affect the mechanical properties, especially flexural strength and compression or tensile strength. However, the effect of Fe_2B and Fe_2Ti on the mechanical properties of TiB_2-Fe cermet is not fully understood with well-controlled microstructures.

Therefore, the aim of this work was to investigate the effect of Ti excess (literally various Ti:B ratio) on the phase composition for those in situ fabricated composites. In order to eliminate the effect of impurities those cermets were fabricated using high purity elemental powders. Similar attempts to modify the matrix phase were emphasized by Azkona et al [4] for Ni-containing TiB_2-based composites, as well as reported recently by Zhang and coworkers [15] for Al-matrix cermets.

The phase composition, microstructure and the properties of SHS products fabricated under pseudo-hot-isostatic pressure conditions (SHS-p-HIP) in a ternary Ti-B-Fe system were characterized. The optimum composition is discussed, considering the relative density, microstructure and hardness. Moreover, mechanical properties for composites with various Ti excess were evaluated quantitatively using bending and compression tests for composites with various phase compositions of the

matrix.

2. Experimental procedure

2.1 Samples preparation

The experiments were carried out with TiB_2-Fe-Ti composites, where a 25 or 35 volume fraction of Fe and various amounts of Ti excess were applied. Commercial powders of titanium (45 μm, purity-99.4%), amorphous boron (0.8 μm, purity-96%), and iron (1-9 μm, purity-99.9%) were used to obtain an initial compact. The chemical compositions of the "green samples" mixtures used for SHS are shown in Table 1, so the intended phase composition of investigated composites is indicated on the ternary phase diagram (Fig.1).

The "green compacts" made of elemental powders were wrapped in graphite foil and then were hermetically closed in steels can. The SHS-p-HIP process was carried out in vacuum furnace (10Pa) situated on universal pressing machine. The SHS reaction was initiated by heating element coiling steel can. The onset of the synthesis was recognized due to the thermocouple attached to the bottom part of the can. After the sudden temperature rise was noticed the pressure was increased form the initial one (20-30MPa) to the final one (150MPa) and held for 5 minutes. Samples were synthesized and densified due to highly exothermic effect associated with TiB_2 synthesis from elemental powders, no additional heating source was used, except for reaction initiation. The samples were cooled down with furnace. The experimental procedure applied in order to prepare composites with various Ti additions was described previously [20, 25].

2.2 Investigation of the sintered samples

The sintered samples were cross-sectioned and polished with diamond dispersive, finally with the grain size of 1μm. The X-ray diffraction (XRD) analysis combined

with Rietveld method was used to determine the phase compositions quantitatively. A scanning electron microscope (SEM) with electron probe microanalyser (EPMA) was applied to observe the microstructure of samples, at the same time a WDS analyzer was used to map the distribution of elements. Transmission electron microscope (TEM) was also employed to confirm phases in the material containing Fe_2B precipitates, based on diffraction patterns. The hardness and microhardness of samples were measured with a Vickers hardness tester under three different loads of 1, 10, or 30kg, respectively. The effect of TiB_2 on the toughness was evaluated by a MOR test, by the 4-point bending technique using rectangular samples 2.5x5.0x25.0mm with outer span lengths of 21.0mm, and crosshead speed of 0.2mm/min, based on the formula described in ASTM: C1161 - 02c standard. Testing forces were applied by means of the mechanical testing machine Instron 5584 with a load capacity of 100kN. The same machine was used for a compression test, where compressive strength was determined using bulk samples 5mmx5mmx10mm in size. Those samples were placed between high strength steel bases and sprayed with h-BN solution lubricant. Both compressive strength and engineering strain were calculated using the ASTM: C1424 - 99 US technical standard.

3. Results and discussion

3.1Microstructure

The composites investigated in this study contained 25 or 35 % vol of Fe, because the previous research [25] indicated that this amount of Fe was optimal in order to achieve high relative density for “in situ” fabricated composites. In each scanning electron image (SEI) the light gray phase corresponds to the Fe-based matrix, while TiB_2 appears as rectangular or hexagonal dark grains which is related to hexagonal structure (P6/mmm, space group 191) of TiB_2. The entirely black small spots correspond to pores. There are also some inclusions in the matrix, but their composition will be discussed with XRD and WDS results. The microstructure of

investigated composites observed using SEM (Fig. 2 and 3) confirmed a good homogeneity and an essentially low porosity.

No significant effect of Ti addition on the TiB_2 grain size in the microstructure was observed. However, the volume fraction of the matrix phase increases at the same time, especially for samples with 35vol% of Fe and a more essential Ti addition (Fig. 3).

As the volume fraction of matrix phase increased, some inhomogeneity demonstrated by wider areas rich in the matrix phase become more common for such “in situ” fabricated composites.

3.2 Phase composition

According to the XRD pattern the TiB_2 was a predominant phase in investigated composites regardless to Ti content, as shown in Fig. 4 and 5. Moreover, each material with Ti deficiency contained Fe_2B co-existing with Fe in the metallic matrix of those cermets.

By setting Ti and B in stoichiometric ratio, which should correspond to a TiB_2 formation (Ti:B molar ratio of 0.500), the formation of an intermetallic Fe_2B phase in the matrix also could not be entirely eliminated. The formation of Fe_2B could be avoided by a Ti excess, and no third phase could be distinguished when the Ti:B atomic ratio was 0.525, while a further Ti addition caused a formation of Fe_2Ti.

Apparently, the position of peaks corresponding to Fe indicated that pure elemental Fe coexisted with a Fe_2B, in the composites with Ti deficiency. However, the Fe shifted peaks in two positions (2Θ = 65 and 82 approximately) indicated a Ti solubility in Fe. As the Ti addition increased (Ti:B at. ratio of 0.525 and 0.566, respectively) the shifted peaks corresponded to $Fe_{0.975}Ti_{0.025}$, or $Fe_{0.964}Ti_{0.036}$ reference patterns, which may indicate a few at. % of Ti, about 2.5at% and 3.6at.% is soluble in the Fe matrix. The phase composition of materials with different Ti:B atomic ratio was determined quantitatively by Rietveld method combined with XRD. For sample with the atomic ratio Ti:B=0.49 66,3% of TiB_2, 26.7% of elemental Fe, and 6.9%

Fe_2B was detected. The (Ti:B) atomic ratio of 0.525 caused only two phases 64,0% of TiB_2 and 36,0% of $Fe_{0.975}Ti_{0.025}$, and the last sample with (Ti:B) atomic ratio of 0.566 contained 64,0% of TiB_2, 26%$Fe_{0.964}Ti_{0.36}$, and 10%Fe_2B. However, it should be emphasized that the accuracy of Rietveld method is relatively good, so the volume contents of phases should be treated semi-quantitatively.

These XRD results are consistent with WDS maps (Fig 6, 8 and 9), as well as diffraction patterns from TEM (Fig. 7).

Multiple precipitations rich in B and Fe could be observed in the matrix of the composite (Fig. 6) with just small deficiency of Ti applied (Ti:B at. ratio of 0.49). Most likely, the precipitations correspond to Fe_2B which could be in compliance to the XRD results. Also diffraction patterns obtained by TEM for the precipitate indicate tetragonal structure (Fig. 7), which should be expected for Fe_2B.

These precipitations were successfully avoided by applying excess Ti, as indicated in the WDS map for the composite with Ti:B, at a ratio of 0.525 (Fig. 8). The matrix phase of the composites consisted of Fe, no Fe_2B was found. Each precipitation which can be distinguished corresponded to small TiB_2 grains which crystallized from a Fe-melt, because it contains both Ti and B. It should be mentioned that the solubility of B in Fe is very low. It is possible that a small amount of Ti (3-4%), comparable to the detection limit by WDS, is dissolved in the Fe-matrix. That could be expected, based on the XRD results. A further Ti addition caused the other intermetallic compound Fe_2Ti to co-precipitate in the Fe matrix (Fig. 9) which could be also expected, based on the phase diagram (Fig.1) and XRD results (Fig.5).

3.3 Hardness

The Vickers hardness of the composites decreased with increasing Ti addition. This effect is caused by a reduced TiB_2 volume fraction as well as by the hardness of phases existing in matrix, Fe, Fe_2B, or Fe_2Ti, and their quantities. The hardness of pure phases, which are constituents in the matrix for investigated composites are $HV_{5.0}$ = 0.3-0.8GPa for Fe; $HV_{1.0}$=15.5GPa for Fe_2B [27], and $HV_{0.0051}$ =12.5GPa for

Fe_2Ti [29]. The last factor which affects the hardness is porosity (P), which based on planimetric measurements was 0.32% for TiB_2-25Fe sample with Ti:B at. Ratio of 0.490; 1.5% in TiB_2-25Fe, where Ti:B = 0.501, 0.9% TiB_2-25Fe, Ti:B = 0.511, and approximately 1.2-1.3% for samples with intended 35vol.% of Fe.

The Vickers microhardness under the load of 1.0kg always exceeded the Vickers hardness under the load of 30 kg. Such effect could be expected due to defects, including porosity and the effect of the matrix, as shown in Fig. 10.

The effect of Ti addition is essential for composites with a intended 25vol.% of Fe, where the initially high hardness 12-16GPa for samples with Ti depletion (Ti:B = 0.49) dropped down to 7-9GPa when the Ti:B ratio increased to 0.511. It should be emphasized that the vol. fraction of TiB_2 decreases due to boron depletion. This indicates that the hardness of TiB_2-25vol.%Fe-xTi is mostly determined by its TiB_2 content. An insignificant effect of Ti excess on the Vickers hardness is observed when the intended volume fraction of Fe increased to 35vol.%. The Vickers hardness for TiB_2-35vol.%Fe-xTi was in general significantly lower (4-6GPa) compared to the previous composites, which was caused by a significant reduction of the hard TiB_2 phase (HV=34.0GPa). However, various Ti excess did not affect the hardness essentially. Relatively small but not negligible effect of matrix phases (Fe, Fe_2B, or Fe_2Ti) is observed for composites when the volume fraction of Fe increased to 35%.

3.4 Mechanical properties

The effect of the matrix phase on the mechanical properties was investigated by means of the MOR test using a 4-points bending technique as well as a compression test. The best flexural strength was obtained for a composite with small Ti excess (Ti:B=0.525) where the only elemental Fe existed in the matrix of MMCs according to the MOR test results (Fig. 11).

Young's modulus of 529 GPa [3] and transverse rupture strength of even 1500 MPa [4] can be reached for nearly monophasic TiB_2 material, while the same properties for unreinforced Fe are E= 210GPa and $\sigma_{0.2}$ = 135MPa, respectively [30].

Despite slightly higher concentration of TiB_2 for a composite with Ti deficiency the flexural strength is reduced and characterized by a higher spread of results (standard deviation as error bars), which means that the matrix phase determines the damping capacity. This behavior confirmed that matrix dislocations are a significant mechanism of damping. Then, both Fe_2B and Fe_2Ti are considered as reinforcing particles. However, intrinsic damping of reinforcing particles, as well as particulate/matrix interface damping are probably minor significance mechanisms. Those results are consistent with previously reported research on TiB_2-reinforced Al-matrix composites [15, 16].

Compressive strength

Compression tests performed for composites containing 35vol.% of Fe and various Ti excess were performed on rectangular samples 5x5x10mm in size. The stress-strain curves (Fig. 12) indicate that the behavior is neither typical for ceramics nor metals, because significant deformation was observed before cracking, while the stress increased rapidly without a clearly recognizable yield point; and rupture occurred suddenly just like for ceramics.

The deformation of all samples before the rupture was relatively small, which is caused by high volume fraction of ceramic TiB_2. Taking into consideration only the investigated samples, the composites with a small Ti deficiency (Ti:B=0.49), which contained Fe_2B coexisting with Fe as a matrix of MMCs, revealed a lower plastic deformation before its fracture. When a significant excess of Ti was used and Fe_2Ti co-existed with Fe as a matrix phase, the smallest deformation was observed. When small Ti excess was applied (Ti:B ratio of 0.525), a better deformation (shrinkage) before fracture was noticed. This composite contained a Fe solid solution with a small amount (3-4%) of Ti, but no Fe-based compounds (neither Fe_2B nor Fe_2Ti) in the matrix of this composite existed. This material exhibited the most ductile behavior, which is expected from cermets.

However, the values of compressive strength indicate that the Ti addition caused a reduced strength in those composites (Fig. 13). A significantly high compressive strength was observed on material with Ti depletion, where Fe_2B co-existed with Fe in

the matrix of the composite. This could be expected, since high hardness (14-15.5GPa) [27, 31] and high compressive stress as high as 1604MPa was reported for Fe_2B layers [31].

The combination of a reduced volume fraction of TiB_2 and the existence of Fe_2Ti are the reasons for a reduced compression strength in the composite fabricated with 0.566 (Ti:B) atomic ratio.

The broken pieces after the compression test revealed cracks propagated in a plane oriented at 45° to the loading direction. Such behavior also indicated ductile behavior according to the maximum shearing strain energy criteria. The microstructure for cracks propagation after a compression test (Fig. 14) as well as after a bending indicated_intergranular mechanism, with cracks depletion, apparently with a particle-matrix debonding and a partial plastic deformation of the metallic matrix.

The particle-matrix debonding was a predominant mechanism for rupture, while the number of cracked TiB_2 grains is small. Similar observations for TiB_2-reinforced Fe-based composites in a fatigue test were reported by Yang and Sinclair [30]. However, the crack propagation probably had started with voids. The microstructure of cracked surface after a compression test is shown on the graph Fig. 15.

The microstructure of the new surface obtained after the compression test indicated no mutual solubility since TiB_2 grains can be easily distinguished from the matrix. The TiB_2 grains appeared like a hexagonal platelet embedded in the Fe-rich matrix. This morphology of TiB_2 is similar to previously reported by Yijie Zhang et al [15]. The deformation of the matrix indicates its ductile behavior, which means that TiB_2 grains were pulled out from the metallic matrix. The composite with a significant Ti addition exhibited the weakest behavior in a bending test and the smallest deformation before rupture, but still the small necks which were formed in the direction perpendicular to the compression force, could be observed on the not entirely ruptured sample (Fig. 16).

The formation of necks perpendicular to the compression direction is caused by tension. It is a well-known phenomenon that, because of tension where tensile force is

oriented outward, the diameter of the material is reduced, so the Poisson ratio can be used to quantitatively describe the effect (Fig. 17).

The formation of necks is observed along the direction of its tension. An exactly inversed effect could be expected for a compression test, where the sample size is reduced in the direction of compression, while tension is expected in the direction perpendicular to the compression. Therefore, the most possible scenario is the formation of necks in the direction perpendicular to compression, where tension occurs.

4. Conclusions

Due to various Ti:B atomic ratios in the TiB_2-based composites from Ti-B-Fe system fabricated “in situ” using elemental powders by means of the SHS-p-HIP technique both phase composition and mechanical properties were essentially modified as follows:

1) The composites with the atomic ratio of Ti:B =0.500 in the powder consisted of three phases: TiB_2, Fe, Fe_2B.
2) Thanks to the excess Ti the formation of unexpected Fe_2B intermetallics in the matrix of those composites was successfully avoided. For instance, by increasing the Ti:B atomic ratio to 0.525 in a composite with an intended 35vol.% of Fe, intermetallics were successfully eliminated. However, further Ti excess (Ti:B ratio of 0.566) leads to the formation of Fe_2Ti.
3) The hardness of the investigated composites was predominantly affected by the volume fraction of TiB_2 grains. Therefore, by increasing the volume fraction of Fe from 25 to 35vol.%, the Vickers hardness decreased more than twice. Considering the same Fe content and effect of a Ti addition, the Vickers hardness became reduced with a decreasing concentration of TiB_2 in two series of investigated composites, however essentially for composites with an intended 25vol.% of Fe.
4) Both bending and compression tests proved ductile behavior of these cermets, manifested by an essential deformation before its rupture, especially for a pure

TiB_2-Fe cermet (Ti:B atomic ratio of 0.525). By producing a pure TiB_2-Fe cermet, the modulus of a rupture was improved, where the highest deformation before its fracture was observed in the compression test, which indicated that either of Fe_2B or Fe_2Ti co-existing with Fe matrix cause reduction in ductility.

5) The highest strength in the compression test possessed composite with matrix phase consisting of Fe and Fe_2B and the highest volume fraction of TiB_2.

Acknowledgements:

The research was partially supported by the Grant for Young and Innovative Researchers (Wakate) from Hokkaido University.

References

[1] Degnan CC, Shipway PH. The incorporation of self-propagating high-temperature synthesis-formed Fe-TiB_2 into ferrous melts. Metall Mater Trans A 2003;33A:2973-83.

[2] Anal A, Bandyopadhyay TK, Das K. Synthesis and characterization of TiB_2-reinforced iron-based composites. J Mater Process Technol 2006;172:70-6.

[3] Zhao G, Huang C, Liu H, Zou B, Zhu H, Wang J. Microstructure and mechanical properties of TiB_2–SiC ceramic composites by Reactive Hot Pressing. Int J Refract Met Hard Mater 2014;42:36-41.

[4] Azkona I, Castro F, Sánchez JM. Abnormal growth of TiB_2 crystals during sintering of TiB_2-Ni_3 (Al, Ti) cemented borides. Metall Mater Trans A 2005;36(2):459-66.

[5] Lee J, Kim NJ, Jung JY, Lee ES, Ahn S. The influence of reinforced particle fracture on strengthening of spray formed Cu-TiB_2 composite. Scr Mater 1998;39(8):1063-9.

[6] Gonzales R, Barandika MG, Ona D, Sanchez JM, Villellas A, Valea A, et al. New binder phases for the consolidation of TiB_2 hardmetals. Mater Sci Eng A 1996;216:185-92.

[7] Wang FC, Zhang ZH, Luo J, Huang CC, Lee SK. A novel rapid route for in situ synthesizing TiB–TiB_2 composites. Compos Sci Technol 2009;69:2682-7.

[8] Ağaoğulları D, Gökçe H, Duman İ, Öveçoğlu ML. Influences of metallic Co and mechanical alloying on the microstructural and mechanical properties of TiB_2 ceramics prepared via pressureless sintering. J Eur Ceram Soc 2012;32:1949-56.

[9] Darabara M, Papadimitriou GD, Bourithis L. Production of Fe–B–TiB_2 metal matrix composites on steel surface. Surf Coat Technol 2006;201:3518-23.

[10] Cobb PC. Titanium carbide as a sintering agent for titanium boride. Mater Des 1990;11(3):156-9.

[11] Li B, Liu Y, Cao H, He L, Li J. Rapid synthesis of TiB_2/Fe composite in situ by spark plasma sintering. J Mater Sci 2009;44: 3909-12.

[12] Ziemnicka-Sylwester M. TiB_2-Based Composites for Ultra-High-Temperature Devices, Fabricated by SHS, Combining Strong and Weak Exothermic Reactions. Mater 2013;6:1903-19.

[13] He L, Liu Y, Li J, Li B. Effects of hot rolling and titanium content on the microstructure and mechanical properties of high boron Fe–B alloys. Mater Des 2012;36:88-93.
[14] Rockwell III T (Ed.). Reactor shielding design manual (No. TID-7004). Division of Reactor Development, Naval Reactors Branch, United States Atomic Energy Commission; 1956.
[15] Zhang Y, Ma N, Wang H, Le Y, Li X. Damping capacity of in situ TiB_2 particulates reinforced aluminium composites with Ti addition. Mater Des 2007;28:628-32.
[16] Zhang J, Perez RJ, Gupta M, Lavernia EJ. Damping behavior of particulate reinforced 2519 Al metal matrix composites. Scr Metall Mater 1993;28:91-6.
[17] Fan T, Yang G, Zhang D. Thermodynamic effect of alloying addition on in-situ reinforced TiB_2/Al composites. Metall Mater Trans A 2005;36A:225-33.
[18] Rajan HM, Ramabalan S, Dinaharan I, Vijay SJ. Synthesis and characterization of in situ formed titanium diboride particulate reinforced AA7075 aluminum alloy cast composites. Mater Des 2013;44:438-45.
[19] Sigl LS, Schwetz KA, Dworak U. Continuous turning with TiB_2 cermets: Preliminary cutting tests. Int J Refract Met Hard Mater 1994;12:95-9.
[20] Ziemnicka-Sylwester M. The Cu matrix cermets remarkably strengthened by TiB_2 “in situ” synthesized via self-propagating high temperature synthesis. Mater Des 2014;53:758-65.
[21] Ziemnicka-Sylwester M. Superhard TiB_2-based composites with different matrix fabricated from elemental powders by SHS-p-HIP. Adv Sci Technol 2013;77:146-52.
[22] Tanaka K, Saito T. Phase equilibria in TiB_2-reinforced high modulus steel. J Phase Equilib 1999;20(3):207-14.
[23] Zhang Z, Shen P, Wang Y, Dong Y, Jiang Q. Fabrication of TiC and TiB2 locally reinforced steel matrix composites using a Fe–Ti–B_4C–C system by an SHS-casting route. J Mater Sci 2007;42: 8350-6.
[24] Lepakova OK, Raskolenko LG, Maksimov YM. Self-propagating high-temperature synthesis of composite material TiB2-Fe. J Mater Sci 2004;39:3723-32
[25] Gai L, Ziemnicka-Sylwester M. The TiB_2-based Fe-matrix composites fabricated using elemental powders in one step process by means of SHS combined with pseudo-HIP. Int J Refract Met Hard Mater 2014;45:141-6.
[26] Prince A, Okamoto H, Villars P (Ed.). Handbook of ternary alloy phase diagrams. ASM international, The Materials Information Society; 1995;5: 5645.
[27] Huang Z, Xing J, Guo C. Improving fracture toughness and hardness of Fe_2 B in high boron white cast iron by chromium addition. Mater Des 2012;31:3084-9.
[28] Ghosh M, Chatterjee S, Mishra B. The effect of intermetallics on the strength properties of diffusion bonds formed between Ti–5.5 Al–2.4 V and 304 stainless steel. Mater Sci Eng A 2003;363:268-74.
[29] Marker MC, Duarte LI, Leinenbach C, Richter KW. Characterization of the Fe-rich corner of Al–Fe–Si–Ti. Intermetallics 2013;39:38-49.
[30] Yang N, Sinclair I. Fatigue crack growth in a particulate TiB_2-reinforced powder metallurgy iron-based composite. Metall Mater Trans A 2003;34A:2017-24.
[31] Rodríguez-Castro G, Campos-Silva I, Chávez-Gutiérrez E, Martínez-Trinidad J, Hernández-Sánchez E, Torres-Hernández A. Mechanical properties of FeB and Fe_2 B layers estimated by Berkovich nanoindentation on tool borided steel. Surf Coat Technol 2013;215:291-9.

List of figures and tables captions

Fe and different Ti:B ratio.

Fig. 14. SEM microstructure of crack profiles (sample surface perpendicular to the fatigue crack growth direction) and associated surrounding microstructure of TiB_2-based Fe-matrix composites with different Ti:Fe ratio: A1, A2) composite with Ti deficiency (Ti:B=0.49); B1, B2) cermet with small Ti excess (Ti:B=0.525), C1, C2) composite with significant Ti addition (Ti:B=0.566)

Fig. 15. New surface after compression test for TiB_2-35vol%Fe composites with different Ti content: no excess Ti (A1, A2, A3), 6vol% of Ti addition, (B1, B2, B3), and 12vol%of excess Ti (C1, C2, C3)

Fig. 16. “Necks” of ductile matrix phase observed in TiB_2-35vol%Fe-12vol%Fe before total sample rupture in compression test: A) near the top surface which was touching pressing holder, B) in the middle of sample, C) near the bottom rammer, D) photography of sample where “necks” were observed (dashed circles), E) photography of other sample indicating mechanisms of fracture (arrows).

Fig. 17. Stress distribution and its consequences to the material: A) tensile test (necking affected by compression perpendicular to tension), B) compression test (barreling caused by tension perpendicular to compression)

Table 1 Compositions of the starting mixtures

	Samples assignation	Ti (at.%)	B (at.%)	Fe (at.%)	Ti:B at.ratio	Ti excess (at.%)
1.	TiB_2-25vol.%Fe	26.55	54.21	19.25	0.490	deficiency
2.	TiB_2-25vol.%Fe-3vol.%Ti	26.97	53.89	19.14	0.501	0.60
3.	TiB_2-25vol.%Fe-6vol.%Ti	27.40	53.58	19.02	0.511	1.18
4.	TiB_2-35vol.%Fe	23.72	48.44	27.84	0.490	deficiency
5.	TiB_2-35vol.%Fe-6vol.%Ti	25.02	47.61	27.37	0.525	1.73
6.	TiB_2-35vol.%Fe-12vol.%Ti	26.44	46.71	26.85	0.566	3.63

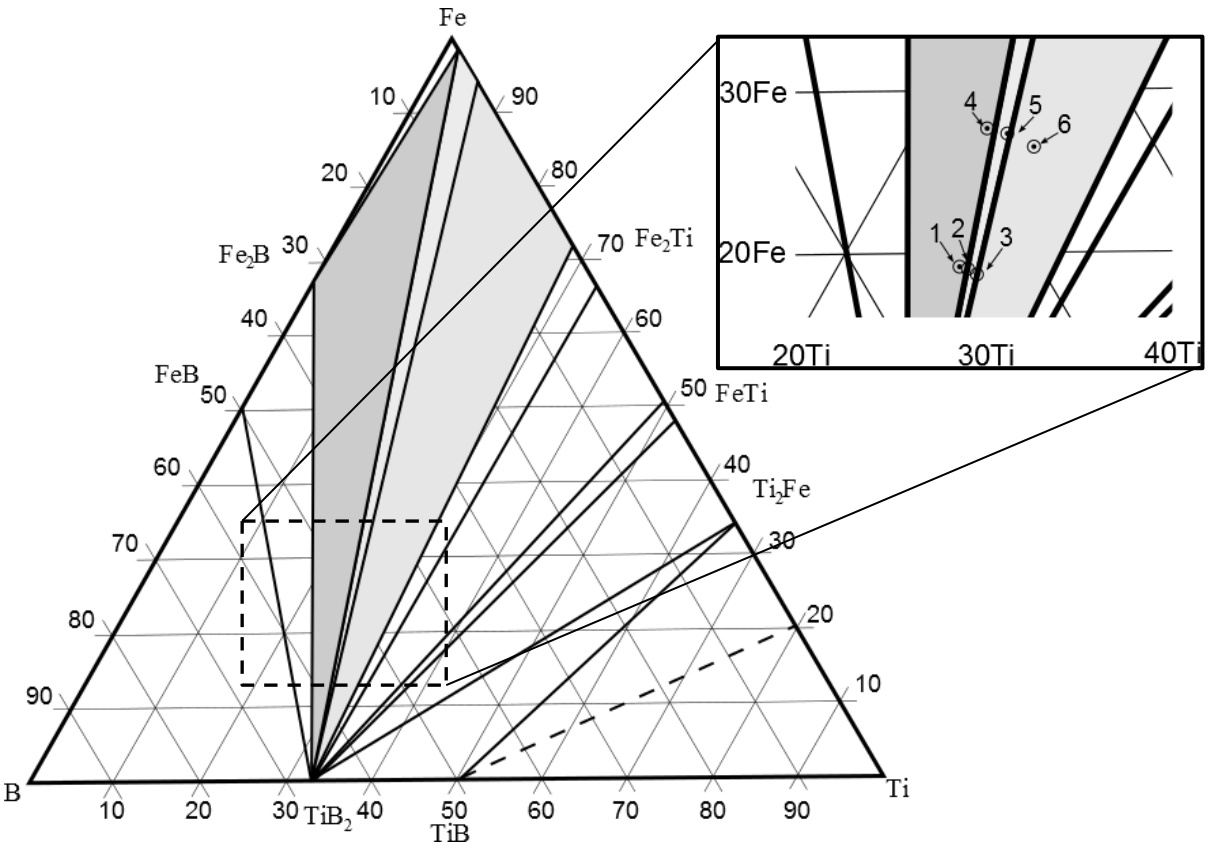

Fig. 1. Isothermal section of ternary Ti-B-Fe system at 1000°C (after Ref. [26]). The enlarged area shows the chemical composition of investigated materials (composition 1-6)

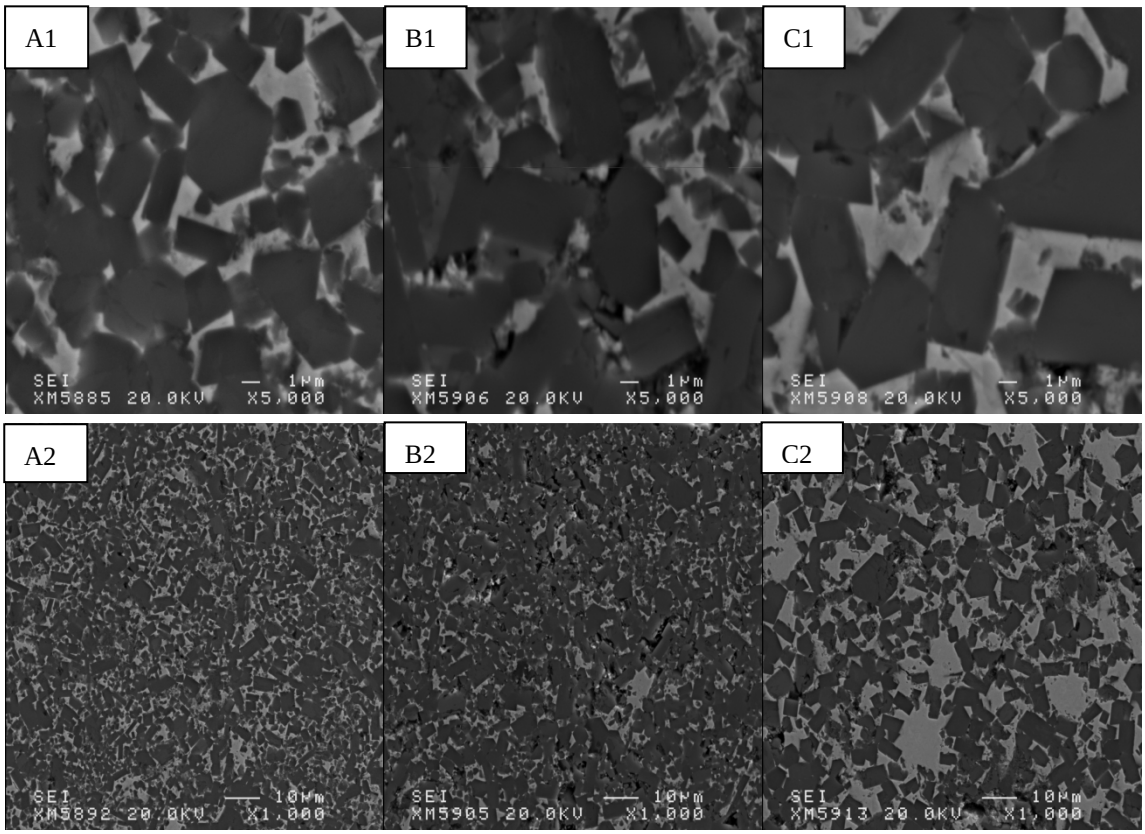

Fig. 2. SEM microstructure (obtained using different magnification) of TiB_2-25Fe composites with different Ti excess: A1, A2) Ti:B = 0.49 (Ti deficiency), B1,B2) Ti:B=0.500, C1,C2) Ti:B=0.511

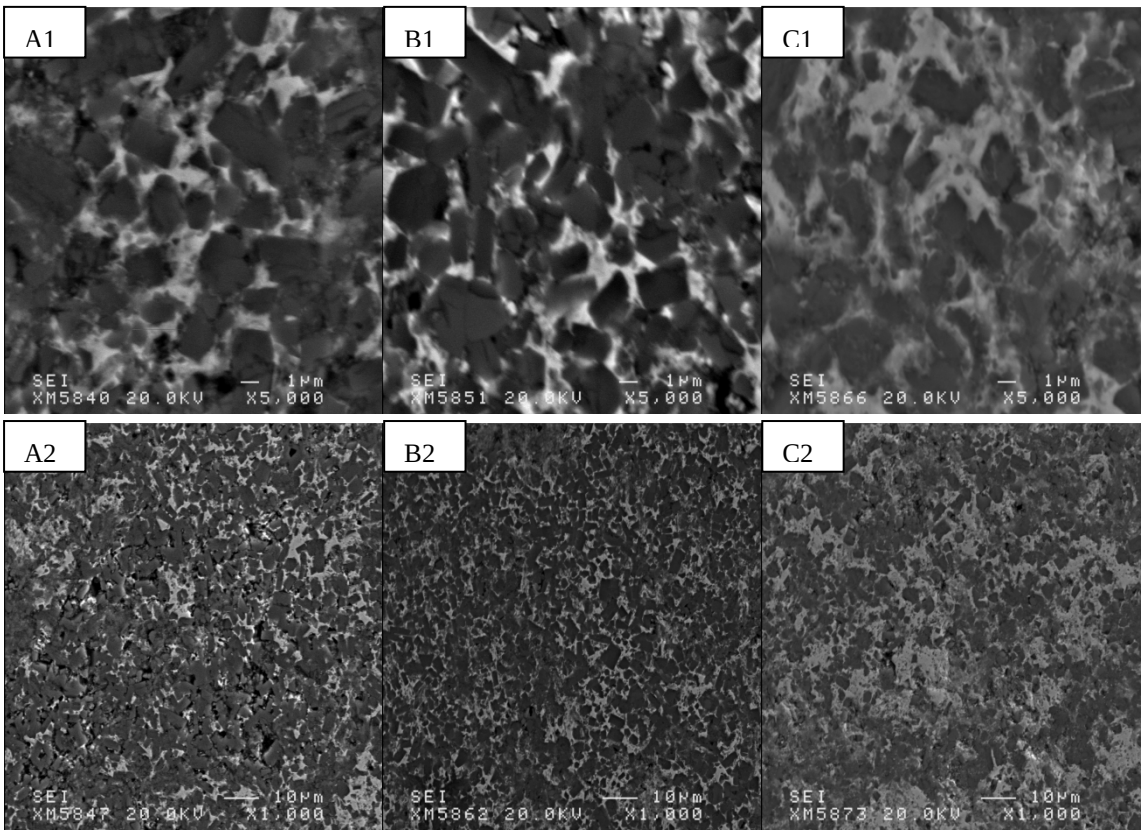

Fig. 3. SEM microstructure of TiB_2-35vol%Fe composites with different Ti:B atomic ratio: A1, A2) Ti:B =0.490 (Ti deficiency); B1, B2) Ti:B = 0.525; C1, C2) Ti:B = 0.566 [at. ratio]

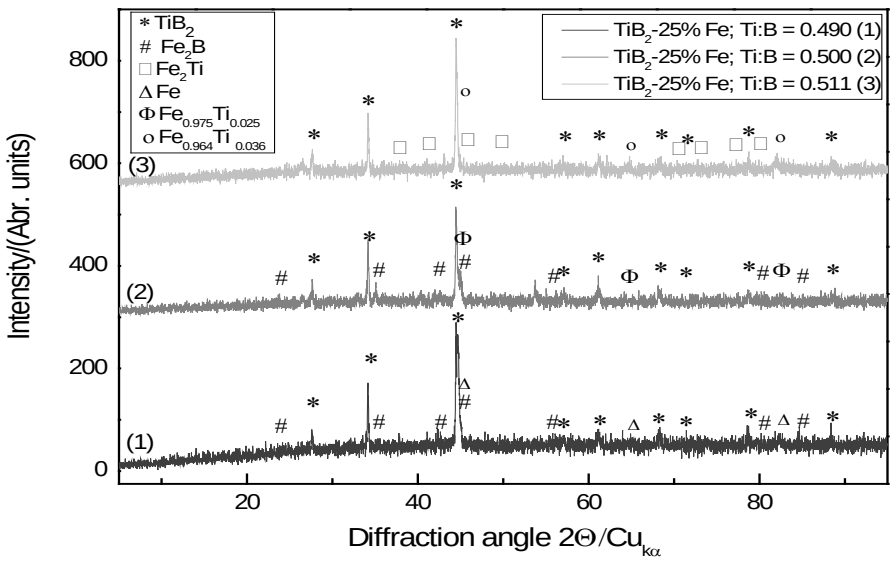

Fig. 4. XRD pattern for TiB_2-25%Fe-xTi composites

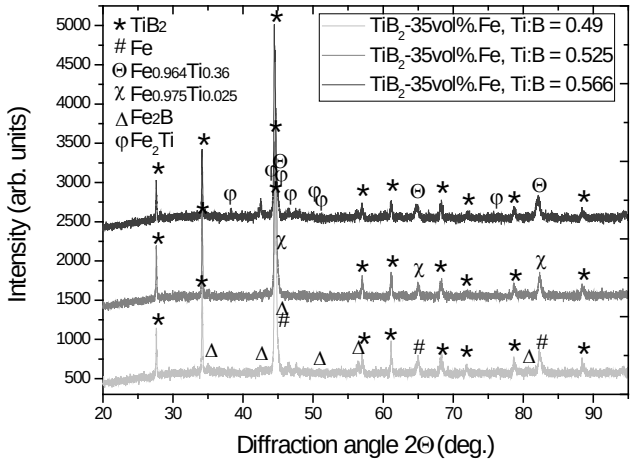

Fig. 5. XRD pattern for 35%Fe-xTi-TiB_2 composites

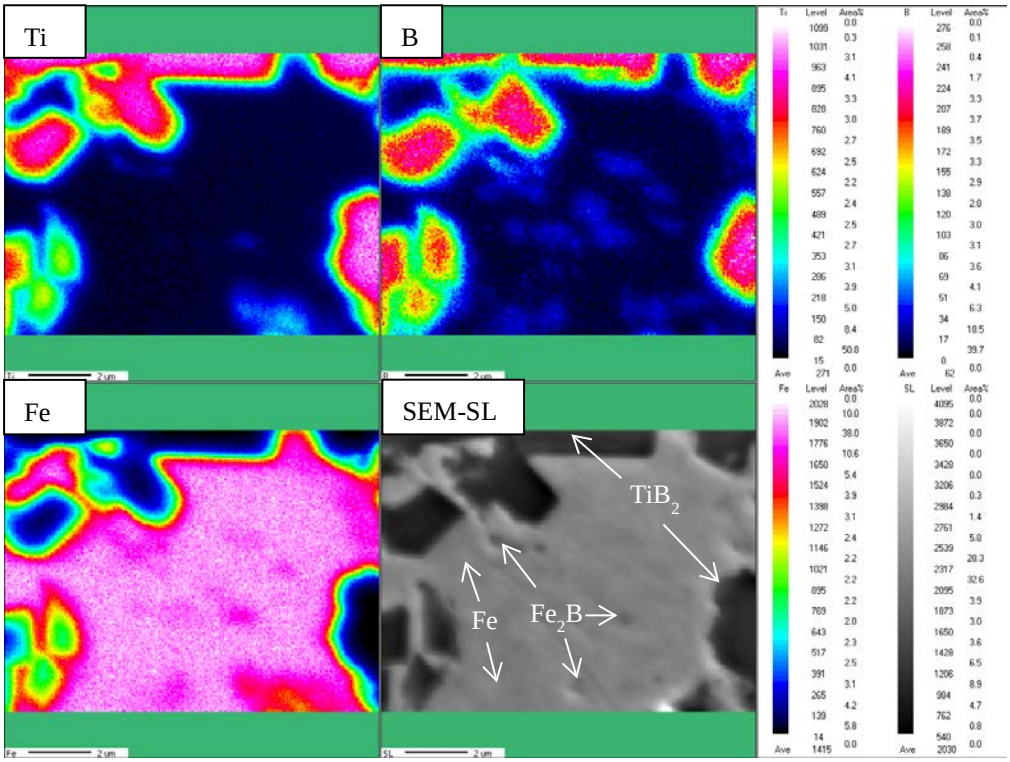

Fig. 6. The WDS map combined with SEM image for matrix-rich area of composites TiB_2-35vol.%Fe with Ti deficiency Ti:B at. ratio of 0.49.

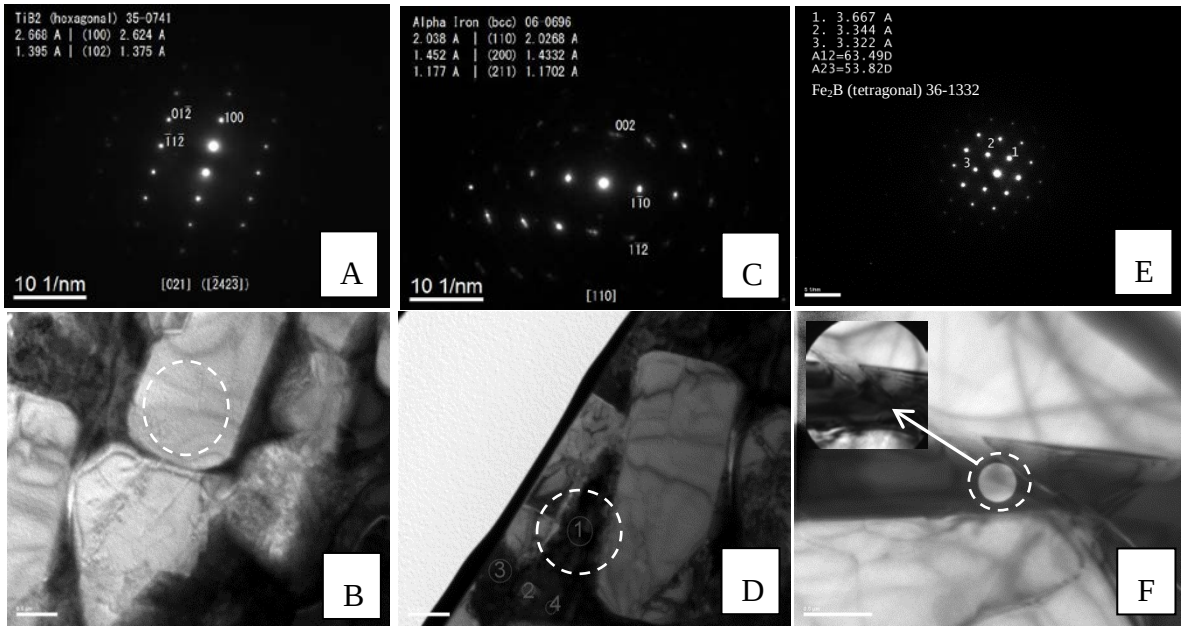

Fig. 7 TEM images and diffraction patterns for phases recognized in TiB_2-35vol%Fe composite with small Ti depletion (Ti:B mol. ratio of 0.49): A) B) TiB_2 grain; C), D) Fe matrix; E, F) Fe_2B precipitate

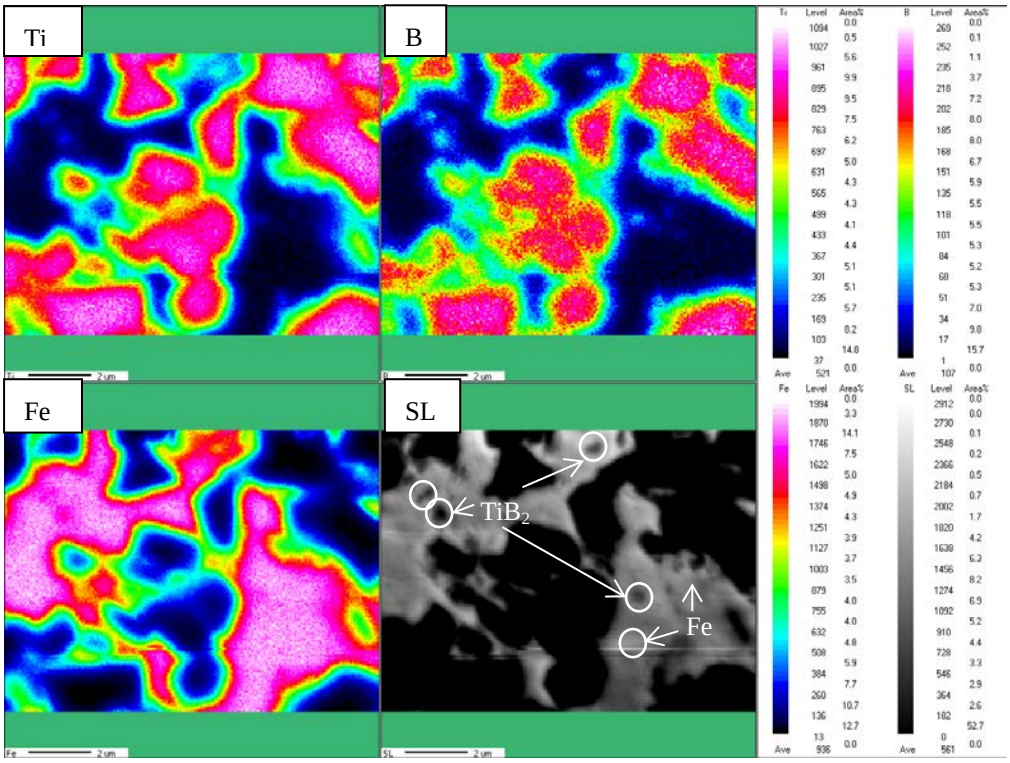

Fig. 8. The WDS map combined with SEM image for matrix-rich area of TiB_2-35vol%Fe composite with Ti:B atomic ratio of 0.525.

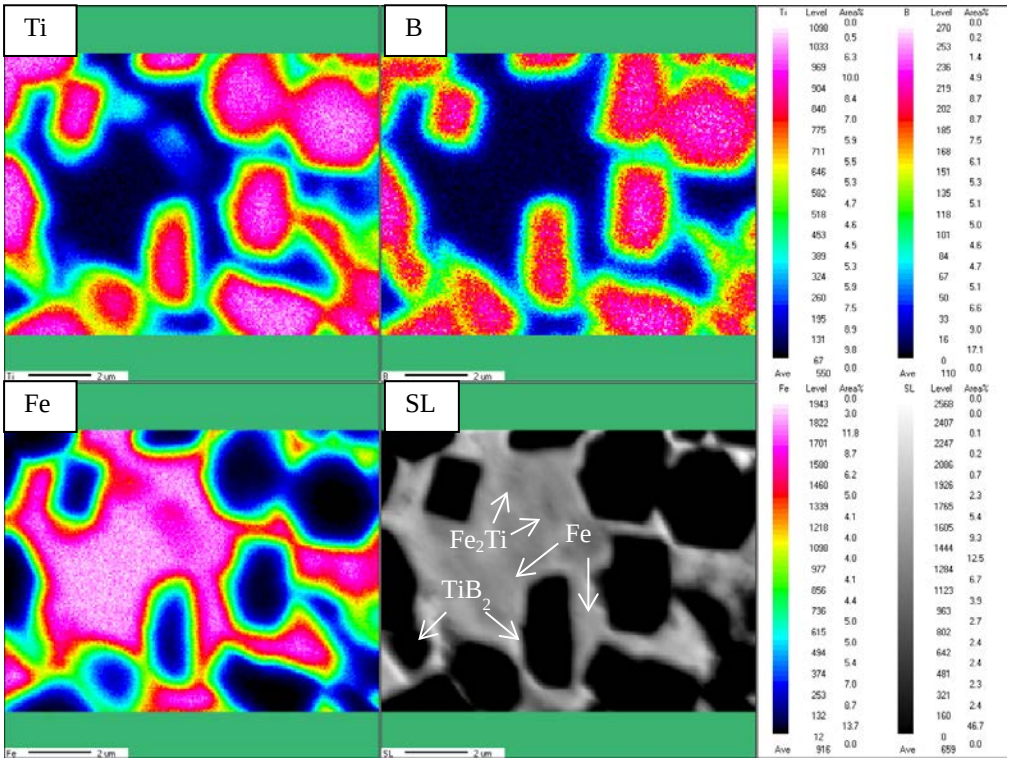

Fig. 9. The WDS map combined with SEM image for matrix-rich area of TiB_2-35vol%Fe composites with significant Ti excess (Ti:B at. ratio of 0.566).

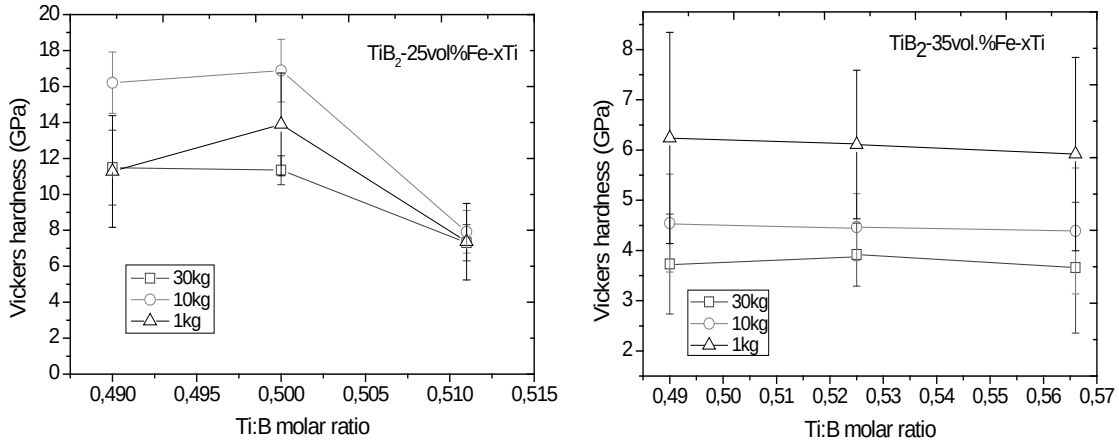

Fig. 10. The Vickers hardness of TiB_2-based composites with various Ti:B atomic ratio containing different Fe content: A) 25vol%Fe, B) 35vol.%Fe

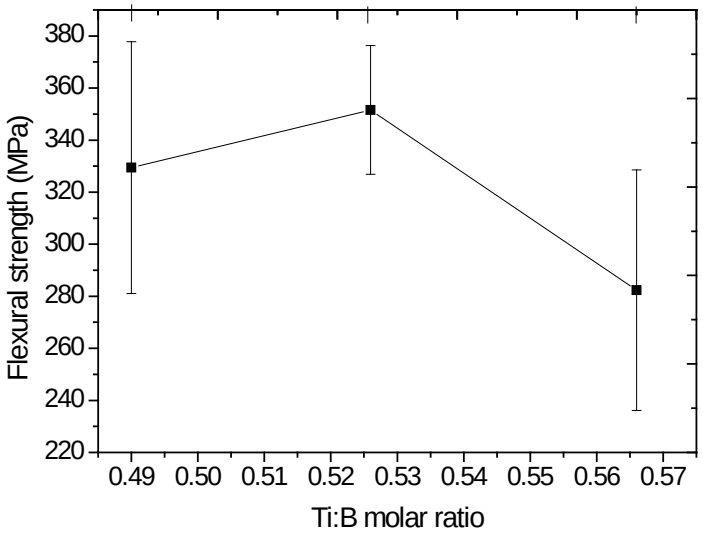

Fig. 11. Effect of matrix phase on the flexural strength in 4-point bending test

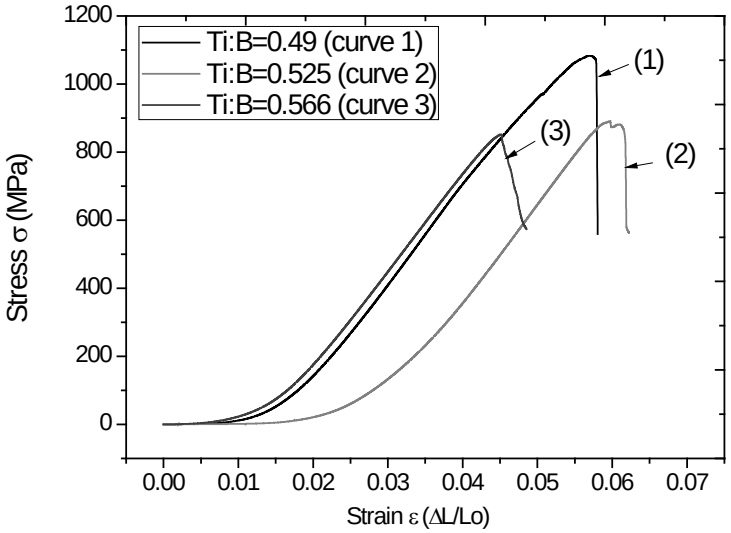

Fig. 12. Stress- strain curves corresponding to compression test for TiB_2-Fe composites with different Ti:B ratio

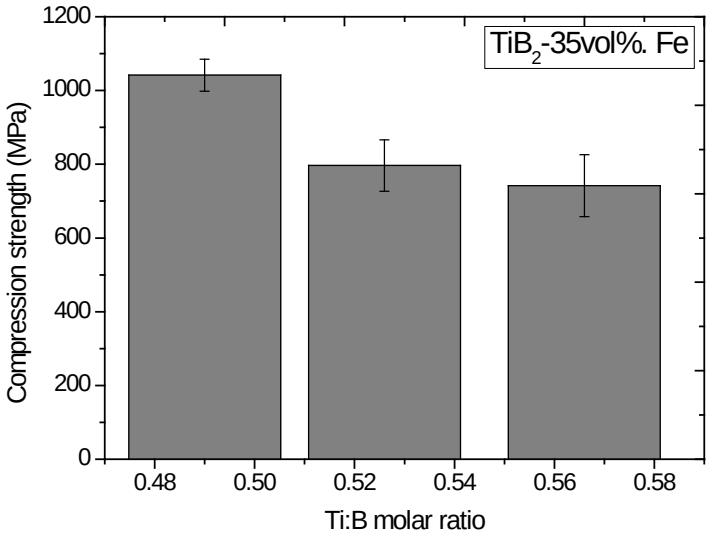

Fig. 13. Compressive strength for TiB_2-Fe composites with intended 35vol% of Fe and different Ti:B ratio.

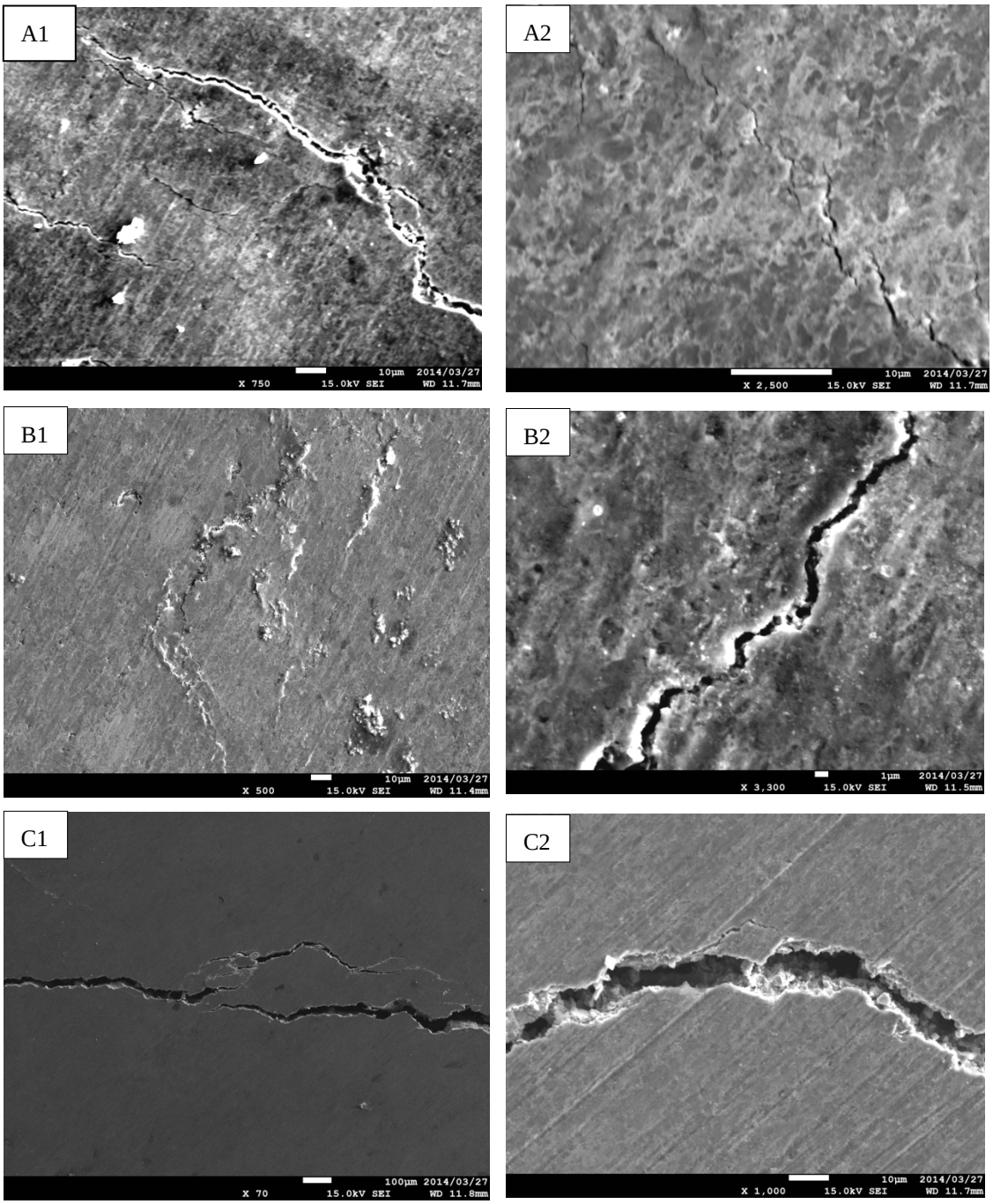

Fig. 14. The SEM microstructure of crack profiles (sample surface perpendicular to the fatigue crack growth direction) and associated surrounding microstructure of TiB_2-based Fe-matrix composites with different Ti:Fe ratio: A1, A2) composite with Ti deficiency (Ti:B=0.49); B1, B2) cermet with small Ti excess (Ti:B=0.525), C1, C2) composite with significant Ti addition (Ti:B=0.566)

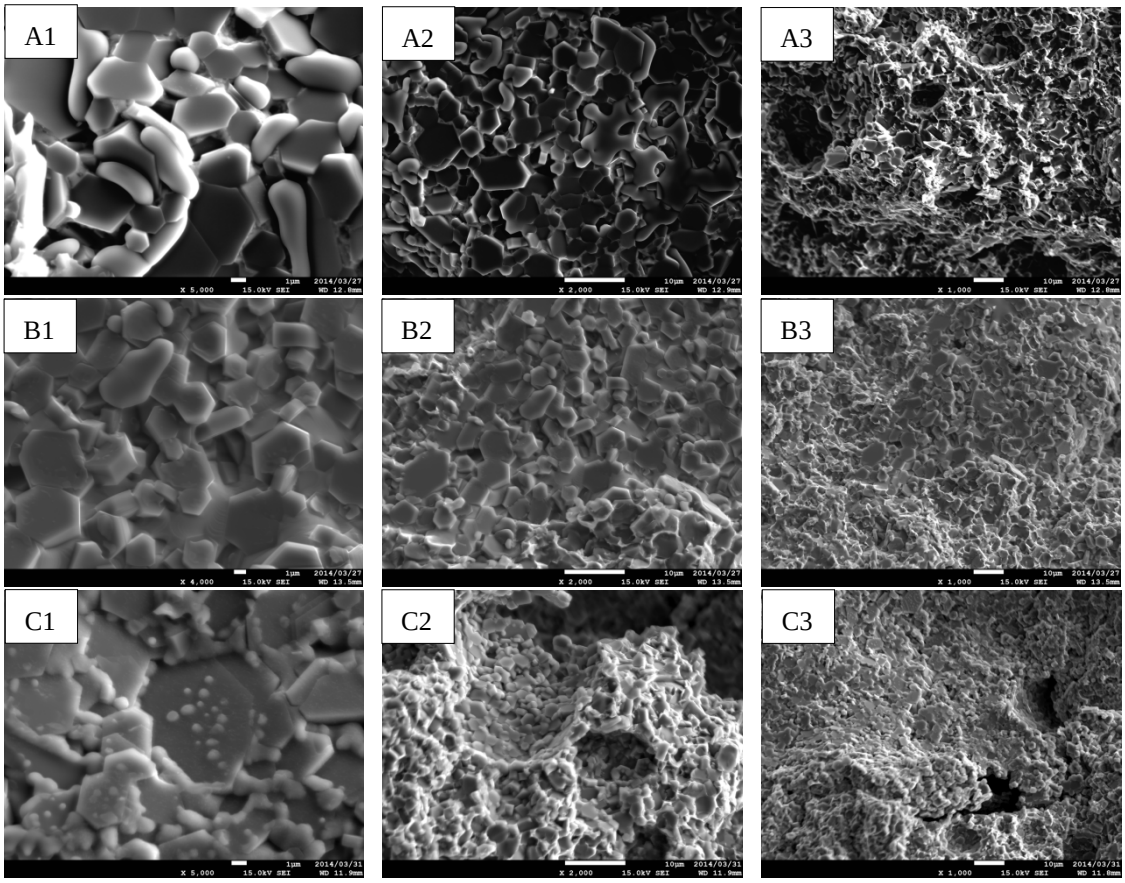

Fig. 15. The new surface after compression test for TiB_2-35vol%Fe composites with different Ti content: no excess Ti (A1, A2, A3), 6vol% of Ti addition, (B1, B2, B3), and 12vol%of excess Ti (C1, C2, C3)

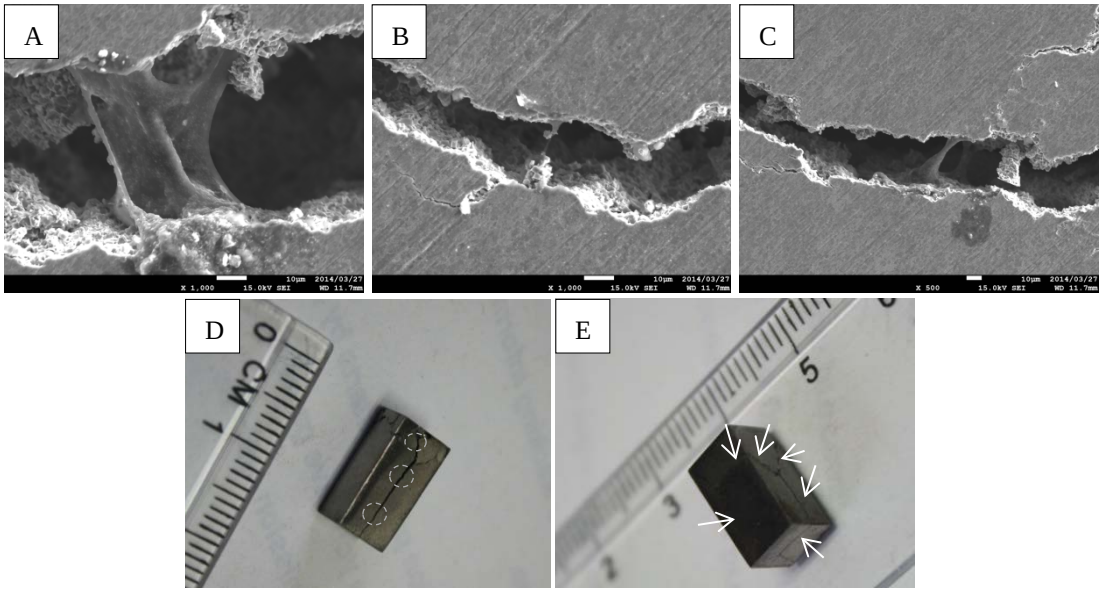

Fig. 16. “Necks” of ductile matrix phase observed in TiB_2-35vol%Fe-12vol%Fe before total sample rupture in compression test: A) near the top surface which was touching pressing holder, B) in the middle of sample, C) near the bottom rammer, D) photography of sample where “necks” were observed (dashed circles), E) photography of other sample indicating mechanisms of fracture (arrows).

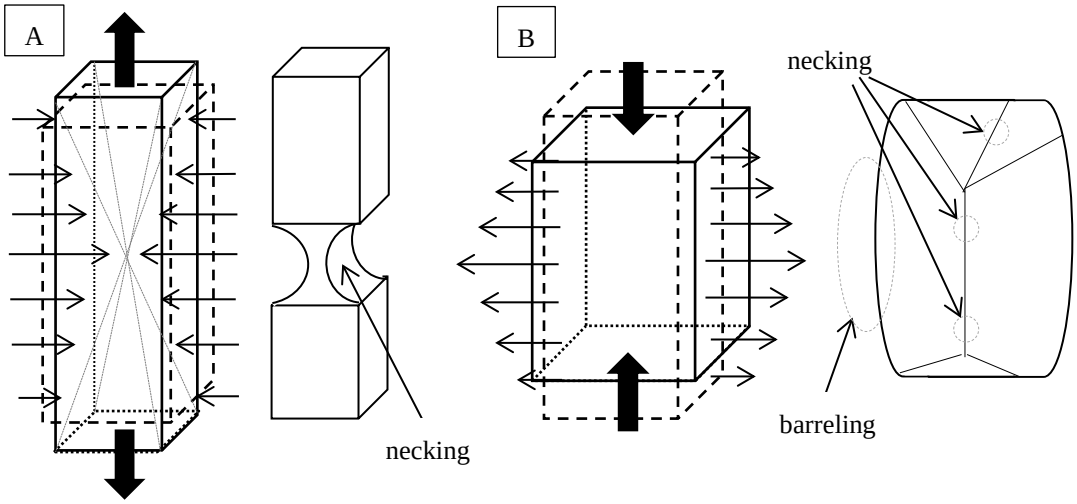

Fig. 17. Stress distribution and its consequences to the material: A) tensile test (necking affected by compression perpendicular to tension), B) compression test (barreling caused by tension perpendicular to compression)